SPE 119084

Stability, Accuracy and Efficiency of Sequential Methods for Coupled Flow and Geomechanics

J. Kim, SPE; H. A. Tchelepi, SPE, Stanford U.; and R. Juanes, SPE, Massachusetts Institute of Technology

This paper was prepared for presentation at the 2009 SPE Reservoir Simulation Symposium held in The Woodlands, Texas, USA, 2–4 February 2009.

Abstract

We perform detailed stability and convergence analyses of sequential-implicit solution methods for coupled fluid flow and reservoir geomechanics. We analyze four different sequential-implicit solution strategies, where each sub-problem (flow and mechanics) is solved implicitly. Two schemes in which the mechanical problem is solved first, namely, the drained and undrained splits, and two schemes, where the flow problem is solved first, namely, the fixed-strain and fixed-stress splits. The Von Neumann method is used to obtain the linear-stability criteria of the four sequential schemes, and numerical simulations are used to test the validity and sharpness of these criteria for representative problems. The analysis indicates that the drained and fixed-strain splits, which are commonly used, are conditionally stable, and that the stability limits depend only on the strength of coupling between flow and mechanics and are independent of the timestep size. So, the drained and fixed-strain schemes cannot be used when the coupling between flow and mechanics is strong. Moreover, numerical solutions obtained using the drained and fixed-strain sequential suffer from oscillations, even when the stability limit is honored. For problems where the deformation may be plastic (nonlinear) in nature, the drained and fixed-strain sequential schemes become unstable when the system enters the plastic regime. On the other hand, the undrained and fixed-stress sequential schemes are unconditionally stable regardless of the coupling strength, and they do not suffer from oscillations. While both the undrained and fixed-stress schemes are unconditionally stable, for the cases investigated we found that the fixed-stress split converges more rapidly than the undrained split. Based on these findings, we strongly recommend the fixed-stress sequential-implicit method for modeling coupled flow and geomechanics in reservoirs.

Introduction

Reservoir geomechanics is concerned with the study of fluid flow and the mechanical response of the reservoir. Reservoir geomechanical behavior plays a critical role in compaction drive, subsidence, well failure, stress dependent permeability, as well as tar sand and heavy oil production (see, e.g., Lewis and Sukirman (1993); Settari and Mourits (1998); Settari and Walters (2001); Thomas et al. (2003); Li and Chalaturnyk (2005); Dean et al. (2006); Jha and Juanes (2007)). The reservoir simulation community has traditionally emphasized flow modeling and oversimplified the mechanical response of the formation through the use of the rock compressibility, taken as a constant coefficient or a simple function of porosity. In order to quantify the deformation and stress fields due to changes in the fluid pressure field and to account for stress dependent permeability effects, rigorous and efficient modeling of the coupling between flow and geomechanics is required.

In recent years, the interactions between flow and geomechanics have been modeled using various coupling schemes (Settari and Mourits, 1998; Settari and Walters, 2001; Mainguy and Longuemare, 2002; Minkoff et al., 2003; Thomas et al., 2003; Tran et al., 2004, 2005; Dean et al., 2006; Jha and Juanes, 2007). Coupling methods are classified into four types: fully coupled, iteratively coupled, explicitly coupled, and loosely coupled (Settari and Walters, 2001; Dean et al., 2006). The characteristics of the coupling methods are:

1. *Fully coupled.* The coupled governing equations of flow and geomechanics are solved simultaneously at every time step. (Lewis and Sukirman, 1993; Wan et al., 2003; Gai, 2004; Phillips and Wheeler, 2007a,b; Jean et al., 2007). For nonlinear problems, an iterative (e.g., Newton–Raphson) scheme is usually employed to compute the numerical solution. The fully coupled method is unconditionally stable, but it is computationally very expensive. Development of a fully coupled flow-mechanics reservoir simulator, which is needed for this approach, is quite costly.

2. *Iteratively coupled.* These are sequential (staggered) solution schemes. Either the flow, or mechanical, problem is solved first, then the other problem is solved using the intermediate solution information (Prevost, 1997; Settari and Mourits,

1998; Settari and Walters, 2001; Mainguy and Longuemare, 2002; Thomas et al., 2003; Tran et al., 2004; Gai, 2004; Tran et al., 2005; Wheeler and Gai, 2007; Jha and Juanes, 2007; Jean et al., 2007). For each time step, several iterations are performed, each involving sequential updating of the flow and mechanics problems until the solution converges to within an acceptable tolerance. For a given time step, at convergence, the fully coupled and sequential solutions are expected to be the same, if they both employ the same spatial discretization schemes of the flow and mechanics problems. In principle, a sequential scheme offers several advantages (Mainguy and Longuemare, 2002), including working with separate modules for flow and mechanics, each with its own advanced numerics and engineering functionality. Sequential treatment also facilitates the use of different computational domains for the flow and mechanical problems. In practice, the domain of the mechanical problem is usually larger than that for flow because the details of the stress and strain fields at reservoir boundaries can be an important part of the problem (Settari and Walters, 2001; Thomas et al., 2003).

3. *Explicitly coupled.* This is also called the non-iterative (single-pass) sequential method. This is a special case of the iteratively coupled method, where only one iteration is taken (Park, 1983; Zienkiewicz et al., 1988; Armero and Simo, 1992; Armero, 1999).

4. *Loosely coupled.* The coupling between the two problems is resolved only after a certain number of flow time steps (Bevillon and Masson, 2000; Gai et al., 2005; Dean et al., 2006; Samier and Gennaro, 2007). This method can be less costly compared with the other strategies. However, reliable estimates of when to update the mechanical response are required.

Given the enormous software development and computational cost of a fully coupled flow–mechanics approach, it is desirable to develop sequential–implicit coupling methods that can be competitive with the fully implicit method (i.e., simultaneous solution of the flow and mechanics problems), in terms of numerical stability and computational efficiency. Sequential, or staggered, coupling schemes offer wide flexibility from a software engineering perspective, and they facilitate the use of specialized numerical methods for dealing with mechanics and flow problems (Felippa and Park, 1980; Settari and Mourits, 1998). As opposed to the fully coupled approach, with sequential-implicit schemes one can use separate software modules for the mechanics and flow problems, whereby the two modules communicate through a well defined interface (Felippa and Park, 1980; Samier and Gennaro, 2007). Then, the robustness and efficiency of each module – flow and geomechanics – are available for the coupled flow-mechanics problem. In order for a sequential-implicit simulation framework to succeed, it should possess stability and convergence properties that are competitive with the corresponding fully coupled strategy.

We analyze the stability and convergence behaviors of sequential (staggered) implicit schemes for coupled mechanics and flow in oil reservoirs. In addition to building on the developments in the reservoir simulation community, we take advantage of the significant efforts in the geotechnical and computational mechanics communities in pursuit of stable and efficient sequential-implicit schemes for coupled poromechanics (or the analogous thermo-mechanics) problems (Park, 1983; Zienkiewicz et al., 1988; Huang and Zienkiewicz, 1998; Farhat et al., 1991; Armero and Simo, 1992; Armero, 1999).

Most of the sequential methods developed in the geotechnical community assume that the mechanical problem is solved first. In this context, two different schemes have been used. One method is called the *drained split* (the isothermal split in the thermo-elastic problem (Armero and Simo, 1992)), and the other one is the *undrained split* (Zienkiewicz et al., 1988; Armero, 1999; Jha and Juanes, 2007) (the adiabatic split in the thermo-elastic problem (Armero and Simo, 1992)). The drained-split scheme freezes the pressure when solving the mechanical deformation problem. This scheme is only conditionally stable, even though each of the sub-problems is solved implicitly (Armero, 1999). The undrained-split strategy, on the other hand, freezes the fluid mass content when solving the mechanics problem. Armero (1999) showed that the undrained split honors the dissipative character of the continuum problem of coupled mechanics and flow in porous media, and that it is unconditionally stable with respect to time evolution, independently of the schemes used for spatial discretization. Of course, numerical solution strategies must employ appropriate spatial discretization schemes for the flow (pressure) and mechanics (displacement vector). The undrained-split scheme has been successfully applied to solve coupled linear (Zienkiewicz et al., 1988; Huang and Zienkiewicz, 1998) and nonlinear (Armero, 1999) problems.

In the reservoir engineering community, the focus has largely been on extending general-purpose (robust behavior with wide engineering functionality) reservoir flow simulators to account for geomechanical deformation effects. As a result, sequential coupling schemes are popular. However, not all sequential coupling schemes are created equal. An obvious split corresponds to freezing the displacements during the solution of the flow problem, and then solving the mechanics problem with the updated pressure field. Unfortunately, this 'fixed-strain' scheme is conditionally stable. Here, we show that the fixed-strain split has stability characteristics that are quite similar to the 'drained' split.

Settari and Mourits (1998) described a sequential-implicit coupling strategy, in which the flow and mechanics problems communicate through a porosity correction. Since then, published simulation results and engineering experience have shown that their method has good stability and convergence properties, especially for linear poroelasticity problems. However, no formal stability analysis of the Settari and Mourits scheme was available. Here, we perform such a stability analysis. Specifically, we show that their scheme is a special case of the 'fixed-stress' split, which we prove to be unconditionally stable. Moreover, we demonstrate that the fixed-stress split is quite effective for nonlinear deformation problems, as well. Wheeler and Gai (2007) employed advanced numerical methods for the spatial discretization of coupled poroelasticity and single-phase flow. Specifically, they used a finite-element method for flow and a continuous Galerkin scheme for the displacement-vector

field. They used a sequential scheme to couple the flow and mechanics problems, in which they first solve the flow problem by lagging the stress field, and then they solve the mechanics problem. Their coupling scheme is quite similar to that used by (Settari and Mourits, 1998) and enjoys good stability properties. Wheeler and Gai (2007) provide a-priori convergence rate estimates of this fixed-stress coupling scheme for single-phase flow and poroelasticity.

Mainguy and Longuemare (2002) described three different strategies to sequentially couple compressible fluid flow in the presence of poroelastic deformation in oil reservoirs. For each sequential strategy, they showed the corresponding 'porosity correction' term that must be used to account for geomechanical effects. Namely, they dervied the porosity correction in terms of (1) volumetric strain, (2) pore volume, and (3) total mean-stress. While no stability analysis of the various sequential schemes was provided, they demonstrated that the pore-compressibility factor can be used as a relaxation parameter to speed up the convergence rate of sequential-implicit schemes (Mainguy and Longuemare, 2002).

There is a growing recognition that different sequential-implicit solution strategies for coupling fluid-flow and geomechanical deformation in reservoirs often lead to vastly different behaviors, in terms of stability, accuracy, and efficiency. Here, we perform detailed analysis of both the stability and convergence properties of the various sequential schemes for coupling flow and geomechanical deformation. Moreover, detailed analysis of the applicability of sequential schemes to coupled nonlinear deformation (e.g., plasticity) and flow is also performed. Specifically, we analyze the stability and convergence behaviors of four sequential coupling schemes: drained, undrained, fixed-strain, and fixed-stress. Both poroelastic and poro-elastoplastic mechanics are analyzed in the presence of a slightly compressible, single-phase fluid.

Our stability analysis shows that the drained and fixed-strain split methods are conditionally stable; moreover, their stability limit is independent of time step size and depends only on the coupling strength. So, problems with strong coupling cannot be solved by the drained or fixed-strain schemes, regardless of the time-step size. On the other hand, we show that the undrained and fixed-stress split methods are unconditionally stable, and that they are free of oscillations with respect to time. We also show that the undrained and fixed-stress sequential-implicit methods are convergent and monotonic for nonlinear elasto-plastic problems.

Mathematical Model

We adopt a classical continuum representation, where the fluid and solid are viewed as overlapping continua. The physical model is based on poroelasticity and poroelastoplasticity theories Coussy (1995). We assume isothermal single-phase flow of a slightly compressible fluid, small deformation (i.e., infinitesimal transformation), isotropic geomaterial, and no stress dependence of flow properties, such as porosity or permeability. The governing equations for coupled flow and reservoir geomechanics come from mass and linear-momentum conservation laws. Under the quasi-static assumption for earth displacements, the governing equation for mechanical deformation of the solid–fluid system can be expressed as

$$\mathrm{Div}\,\boldsymbol{\sigma} + \rho_b \boldsymbol{g} = \mathbf{0}, \tag{1}$$

where $\mathrm{Div}(\cdot)$ is the divergence operator, $\boldsymbol{\sigma}$ is the Cauchy total stress tensor, $\boldsymbol{g}$ is the gravity vector, $\rho_b = \phi\rho_f + (1-\phi)\rho_s$ is the bulk density, ρ_f is fluid density, ρ_s is the density of the solid phase, and ϕ is the true porosity. The true porosity is defined as the ratio of the pore volume and the bulk volume in the deformed configuration. A stress–strain relation must be specified for the mechanical behavior of the porous medium. Changes in total stress and fluid pressure are related to changes in strain and fluid content by Biot's theory (Biot, 1941; Geertsma, 1957; Coussy, 1995; Lewis and Schrefler, 1998; Borja, 2006). Following Coussy (1995), the poroelasticity equations can be written as

$$\boldsymbol{\sigma} - \boldsymbol{\sigma}_0 = \mathbf{C}_{dr} : \boldsymbol{\varepsilon} - b(p - p_0)\mathbf{1}, \tag{2}$$

$$\frac{1}{\rho_{f,0}}(m - m_0) = b\varepsilon_v + \frac{1}{M}(p - p_0), \tag{3}$$

where subscript 0 refers to the reference state, $\mathbf{C}_{dr}$ is the rank-4 drained elasticity tensor, $\mathbf{1}$ is the rank-2 identity tensor, p is fluid pressure, m is fluid mass per unit bulk volume, M is the Biot modulus, and b is the Biot coefficient. Note that we use the convention that tensile stress is positive. Assuming that the infinitesimal transformation assumption is applicable, the linearized strain tensor, $\boldsymbol{\varepsilon}$, can be expressed as

$$\boldsymbol{\varepsilon} = \mathbf{Grad}^s\, \boldsymbol{u} = \frac{1}{2}(\mathbf{Grad}\, \boldsymbol{u} + \mathbf{Grad}^t\, \boldsymbol{u}). \tag{4}$$

Note that (Coussy, 1995)

$$\frac{1}{M} = \phi_0 c_f + \frac{b - \phi_0}{K_s}, \tag{5}$$

$$b = 1 - \frac{K_{dr}}{K_s}, \tag{6}$$

where c_f is the fluid compressibility ($1/K_f$), K_f is the bulk modulus of the fluid, K_s is the bulk modulus of the solid grain, and K_{dr} is the drained bulk modulus. The strain and stress tensors can be expressed in terms of their volumetric and deviatoric

parts as follows:

$$\boldsymbol{\varepsilon} = \frac{1}{3}\varepsilon_v \mathbf{1} + \boldsymbol{e}, \tag{7}$$

$$\boldsymbol{\sigma} = \sigma_v \mathbf{1} + \boldsymbol{s}, \tag{8}$$

where $\varepsilon_v = \mathrm{tr}\boldsymbol{\varepsilon}$ is the volumetric strain (trace of the strain tensor), $\boldsymbol{e}$ is the deviatoric part of the strain tensor, $\sigma_v = \frac{1}{3}\mathrm{tr}\boldsymbol{\sigma}$ is the volumetric (mean) total stress, and $\boldsymbol{s}$ is the deviatoric total stress tensor.

Under the assumption of small deformations, the fluid mass conservation equation is

$$\frac{\partial m}{\partial t} + \mathrm{Div}\, \boldsymbol{q} = \rho_{f,0} f, \tag{9}$$

where $\boldsymbol{q}$ is the fluid mass flux, and f is a volumetric source term. The fluid volume flux (velocity), $\boldsymbol{v} = \boldsymbol{q}/\rho_{f,0}$, relative to the deforming skeleton, is given by Darcy's law (Coussy, 1995):

$$\boldsymbol{v} = -\frac{1}{B_f}\frac{\boldsymbol{k}}{\mu}(\mathbf{Grad}\, p - \rho_f \boldsymbol{g}), \tag{10}$$

where $\boldsymbol{k}$ is the absolute permeability tensor, μ is fluid viscosity, and $B_f = \rho_{f,0}/\rho_f$ is the formation volume factor of the fluid (Aziz and Settari, 1979).

Using Equation 3, we write Equation 9 in terms of pressure and volumetric strain:

$$\frac{1}{M}\frac{\partial p}{\partial t} + b\frac{\partial \varepsilon_v}{\partial t} + \mathrm{Div}\, \frac{\boldsymbol{q}}{\rho_{f,0}} = f. \tag{11}$$

By noting the relation between volumetric stress and strain,

$$(\sigma_v - \sigma_{v,0}) + b(p - p_0) = K_{dr}\varepsilon_v, \tag{12}$$

we write Equation 11 in terms of pressure and the total (mean) stress,

$$\left(\frac{1}{M} + \frac{b^2}{K_{dr}}\right)\frac{\partial p}{\partial t} + \frac{b}{K_{dr}}\frac{\partial \sigma_v}{\partial t} + \mathrm{Div}\, \frac{\boldsymbol{q}}{\rho_{f,0}} = f. \tag{13}$$

Equations 11 and 13 are two equivalent expressions of mass conservation (i.e., flow problem) in a deforming porous medium. Substitution of Darcy's law in Equations 11 and 13 leads, respectively, to pressure-strain and pressure-stress forms of the flow equation. The two forms of mass conservation are equivalent. However, using one form versus the other in a sequential-implicit scheme to couple flow with mechanics leads to very different stability and convergence behaviors. Later, we use these expressions (Eqs. 11 and 13) to show the exact forms of the operator-splitting strategies (solving two sub-problems - flow and mechanics - sequentially) studied in this paper.

To complete the description of the coupled flow and geomechanics mathematical problem, we need to specify initial and boundary conditions. For the flow problem, we consider the boundary conditions $p = \bar{p}$ (prescribed pressure) on Γ_p, and $\boldsymbol{v}\cdot\boldsymbol{n} = \bar{v}$ (prescribed volumetric flux) on Γ_v, where $\boldsymbol{n}$ is the outward unit normal to the boundary, $\partial\Omega$. For well-posedness, we assume that $\Gamma_p \cap \Gamma_v = \emptyset$, and $\Gamma_p \cup \Gamma_v = \partial\Omega$.

The boundary conditions for the mechanical problem are $\boldsymbol{u} = \bar{\boldsymbol{u}}$ (prescribed displacement) on Γ_u and $\boldsymbol{\sigma}\cdot\boldsymbol{n} = \bar{\boldsymbol{t}}$ (prescribed traction) on Γ_σ. Again, we assume $\Gamma_u \cap \Gamma_\sigma = \emptyset$, and $\Gamma_u \cup \Gamma_\sigma = \partial\Omega$.

Initialization of the geomechanical model is a difficult task in itself (Fredrich et al., 2000). The initial stress field should satisfy mechanical equilibrium, and be consistent with the history of the stress-strain paths. Here, we take the initial condition of the coupled problem as $p|_{t=0} = p_0$ and $\boldsymbol{\sigma}|_{t=0} = \boldsymbol{\sigma}_0$.

Discretization

The finite-volume method is widely used in reservoir flow simulation community (Aziz and Settari, 1979). On the other hand, nodal-based finite-element methods are quite popular in the geotechnical engineering and thermomechanics communities (Zienkiewicz et al., 1988; Lewis and Sukirman, 1993; Lewis and Schrefler, 1998; Armero and Simo, 1992; Armero, 1999; Wan et al., 2003; White and Borja, 2008). In the finite-volume method for the flow problem, the pressure is located at the cell center. In the nodal-based finite-element method for the mechanical problem, the displacement vector is located at vertices (Hughes, 1987). This space discretization strategy has the following characteristics: local mass conservation at the element level, a continuous displacement field, which allows for tracking the deformation, and convergent approximations with the lowest-order discretization (Jha and Juanes, 2007). Since we assume a slightly compressible fluid, the given space discretization provides a stable pressure field (Phillips and Wheeler, 2007a,b). It is well known that for incompressible (solid-fluid) systems, nodal based finite-element methods incur spurious pressure oscillations if equal-order approximations of pressure and displacement (e.g.,

piecewise continuous interpolation) are used (Vermeer and Verruijt, 1981; Murad and Loula, 1992, 1994; White and Borja, 2008). Stabilization techniques for such spurious pressure oscillations have been studied by several authors (Murad and Loula, 1992, 1994; Wan, 2002; Truty and Zimmermann, 2006; White and Borja, 2008).

We partition the domain into nonoverlapping elements (grid blocks), $\Omega = \cup_{j=1}^{n_{\text{elem}}} \Omega_j$, where n_{elem} is the number of elements. Let $\mathcal{Q} \subset L^2(\Omega)$ and $\mathcal{U} \subset (H^1(\Omega))^d$ (where $d = 2, 3$ is the number of space dimensions), be the functional spaces of the solution for pressure, p, and displacements, $\boldsymbol{u}$. Let $\mathcal{Q}_0$ and $\mathcal{U}_0$ be the corresponding function spaces for the test functions φ and $\boldsymbol{\eta}$, for flow and mechanics, respectively (Jha and Juanes, 2007), and let $\mathcal{Q}_h$, $\mathcal{Q}_{h,0}$, $\mathcal{U}_h$ and $\mathcal{U}_{h,0}$ be the corresponding finite-dimensional subspaces. Then, the discrete approximation of the weak form of the governing equations 1 and 9 becomes: Find $(\boldsymbol{u}_h, p_h) \in \mathcal{U}_h \times \mathcal{Q}_h$ such that

$$\int_\Omega \mathbf{Grad}^s \boldsymbol{\eta}_h : \boldsymbol{\sigma}_h \, d\Omega = \int_\Omega \boldsymbol{\eta}_h \cdot \rho_b \boldsymbol{g} \, d\Omega + \int_{\Gamma_\sigma} \boldsymbol{\eta}_h \cdot \bar{\boldsymbol{t}} \, d\Gamma \quad \forall \boldsymbol{\eta}_h \in \mathcal{U}_{h,0}, \tag{14}$$

$$\frac{1}{\rho_{f,0}} \int_\Omega \varphi_h \frac{\partial m_h}{\partial t} \, d\Omega + \int_\Omega \varphi_h \operatorname{Div} \boldsymbol{v}_h \, d\Omega = \int_\Omega \varphi_h f \, d\Omega, \quad \forall \varphi_h \in \mathcal{Q}_{h,0}. \tag{15}$$

The pressure and displacement fields are approximated as follows:

$$p_h = \sum_{j=1}^{n_{\text{elem}}} \varphi_j P_j, \tag{16}$$

$$\boldsymbol{u}_h = \sum_{b=1}^{n_{\text{node}}} \eta_b \boldsymbol{U}_b, \tag{17}$$

where n_{node} is the number of nodes, P_j are the element pressures, and $\boldsymbol{U}_b$ are the displacement vectors at the element nodes (vertices).

We restrict our analysis to pressure shape-functions that are piecewise constant, so that φ_j takes a constant value of 1 over element j and 0 at all other elements. Therefore, Equation 15 can be interpreted as a mass conservation statement element-by-element. The second term can be integrated by parts to arrive at the sum of integral fluxes, $V_{h,ij}$, between element i and its adjacent elements j:

$$\int_\Omega \varphi_i \operatorname{Div} \boldsymbol{v}_h \, d\Omega = -\int_{\partial\Omega_i} \boldsymbol{v}_h \cdot \boldsymbol{n}_i \, d\Gamma = -\sum_{j=1}^{n_{\text{face}}} \int_{\Gamma_{ij}} \boldsymbol{v}_h \cdot \boldsymbol{n}_i \, d\Gamma = -\sum_{j=1}^{n_{\text{face}}} V_{h,ij}. \tag{18}$$

The inter-element flux can be evaluated using a two-point, or a multipoint, flux approximation (Aavatsmark, 2002).

The displacement interpolation functions are the usual C^0-continuous isoparametric functions, such that η_b takes a value of 1 at node b, and 0 at all other nodes. Inserting the interpolation from Equations 16–17, and testing Equations 14–15 against each individual shape function, the semi-discrete finite-element/finite-volume equations can be written as:

$$\int_\Omega \boldsymbol{B}_a^T \boldsymbol{\sigma}_h \, d\Omega = \int_\Omega \eta_a \rho_b \boldsymbol{g} \, d\Omega + \int_{\Gamma_\sigma} \eta_a \bar{\boldsymbol{t}} \, d\Gamma \quad \forall a = 1, \ldots, n_{\text{node}}, \tag{19}$$

$$\int_{\Omega_i} \frac{1}{M} \frac{\partial P_i}{\partial t} \, d\Omega + \int_{\Omega_i} b \frac{\partial \varepsilon_v}{\partial t} \, d\Omega - \sum_{j=1}^{n_{\text{face}}} V_{h,ij} = \int_{\Omega_i} f \, d\Omega, \quad \forall i = 1, \ldots, n_{\text{elem}}, \tag{20}$$

where Equation 20 is obtained from Equations 3, 15, and 18.

The matrix $\boldsymbol{B}_a$ is the linearized strain operator, which in 2D takes the form

$$\boldsymbol{B}_a = \begin{bmatrix} \partial_x \eta_a & 0 \\ 0 & \partial_y \eta_a \\ \partial_y \eta_a & \partial_x \eta_a \end{bmatrix}. \tag{21}$$

The stress and strain tensors are expressed in compact engineering notation (Hughes, 1987). For example, in 2D,

$$\boldsymbol{\sigma}_h = \begin{bmatrix} \sigma_{h,xx} \\ \sigma_{h,yy} \\ \sigma_{h,xy} \end{bmatrix}, \qquad \boldsymbol{\varepsilon}_h = \begin{bmatrix} \varepsilon_{h,xx} \\ \varepsilon_{h,yy} \\ 2\varepsilon_{h,xy} \end{bmatrix}. \tag{22}$$

The stress–strain relation for linear poroelasticity takes the form:

$$\boldsymbol{\sigma}_h = \boldsymbol{\sigma}'_h - b p_h \mathbf{1}, \qquad \delta \boldsymbol{\sigma}'_h = \boldsymbol{D} \delta \boldsymbol{\varepsilon}_h, \tag{23}$$

where $\boldsymbol{\sigma}'$ is the effective stress tensor, and $\boldsymbol{D}$ is the elasticity matrix which, for 2D plane strain conditions, reads:

$$\boldsymbol{D} = \frac{E(1-\nu)}{(1+\nu)(1-2\nu)} \begin{bmatrix} 1 & \frac{\nu}{1-\nu} & \frac{\nu}{1-\nu} \\ \frac{\nu}{1-\nu} & 1 & \frac{\nu}{1-\nu} \\ \frac{\nu}{1-\nu} & \frac{\nu}{1-\nu} & 1 \end{bmatrix}, \tag{24}$$

where E is Young's modulus, and ν is Poisson's ratio.

The coupled equations of quasi-static poromechanics form an elliptic–parabolic system of equations. A fully discrete system of equations can be obtained by further discretizing in time the mass accumulation term in Equations 19–20. Throughout this paper, the backward Euler method is used for time discretization.

Solution Strategies

A primary objective of this work is to analyze the stability of sequential-implicit solution schemes for coupled flow and mechanics in porous media, where the two problems of flow and mechanics are solved in sequence such that each problem is solved using implicit time discretization. We analyze four sequential-implicit solution strategies, namely, drained, undrained, fixed-strain, and fixed-stress. Because we use the fully coupled scheme as reference, we also summarize its stability property.

The drained and undrained splits solve the mechanical problem first, and then they solve the fluid-flow problem (left diagram of Figure 1). In contrast, the fixed-strain and fixed-stress splits solve for the fluid flow problem first, and then they solve the mechanical problem (right diagram of Figure 1).

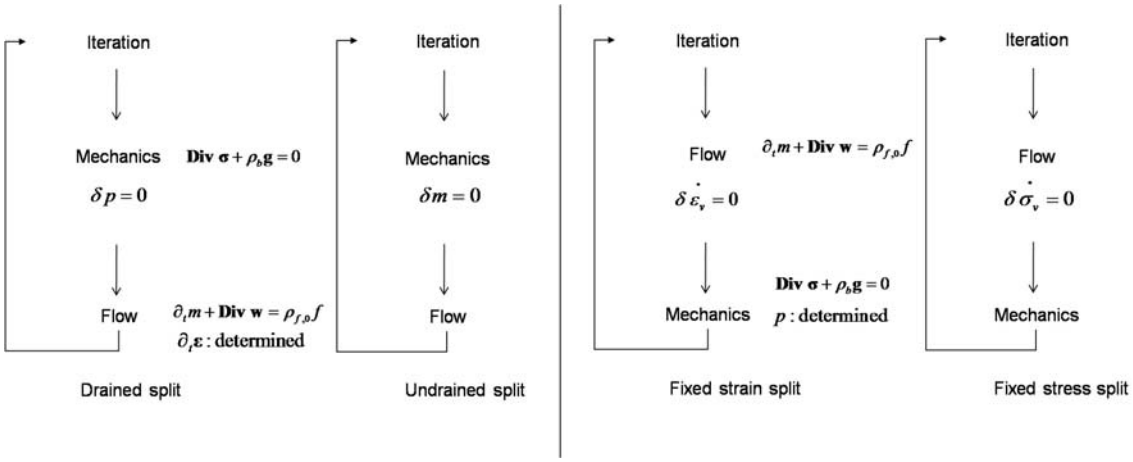

Figure 1: Iteratively coupled methods for flow and geomechanics. Left figure: drained and undrained split methods. Right figure: fixed-strain and fixed-stress split methods. The symbol $\dot{(\,)}$ denotes time derivative, $\partial(\,)/\partial t$.

Fully Coupled Method. Let us denote by $\mathcal{A}$ the operator of the original problem (Equations 1 and 9). The discrete approximation of this operator corresponding to the fully coupled method can be represented as:

$$\begin{bmatrix} \boldsymbol{u}^n \\ \boldsymbol{p}^n \end{bmatrix} \xrightarrow{\mathcal{A}_{fc}} \begin{bmatrix} \boldsymbol{u}^{n+1} \\ \boldsymbol{p}^{n+1} \end{bmatrix}, \quad \text{where} \quad \mathcal{A}_{fc} : \begin{cases} \operatorname{Div} \boldsymbol{\sigma} + \rho_b \boldsymbol{g} = \boldsymbol{0}, \\ \dot{m} + \operatorname{Div} \boldsymbol{q} = \rho_{f,0} f, \end{cases} \tag{25}$$

where $\dot{(\,)}$ denotes time derivative. Using a backward Euler time discretization in Equations 19 and 20, the residual form of the fully-discrete coupled equations is:

$$\boldsymbol{R}_a^u = \int_\Omega \boldsymbol{B}_a^T \boldsymbol{\sigma}_h^{n+1} \, d\Omega - \int_\Omega \eta_a \rho_b^{n+1} \boldsymbol{g} \, d\Omega - \int_{\Gamma_\sigma} \eta_a \bar{\boldsymbol{t}}^{n+1} \, d\Gamma \quad \forall a = 1, \ldots, n_{\text{node}}, \tag{26}$$

$$R_i^p = \int_{\Omega_i} \frac{1}{M} (P_i^{n+1} - P_i^n) \, d\Omega + \int_{\Omega_i} b(\varepsilon_v^{n+1} - \varepsilon_v^n) \, d\Omega - \Delta t \sum_{j=1}^{n_{\text{face}}} V_{h,ij}^{n+1} - \Delta t \int_{\Omega_i} f^{n+1} \, d\Omega \quad \forall i = 1, \ldots, n_{\text{elem}}. \tag{27}$$

where $\boldsymbol{R}_a^u$ and R_i^p are the residuals for mechanics (node a) and flow (element i), respectively. The superscript n indicates the time level. The set of Equations 26–27 is to be solved for the nodal displacements $\boldsymbol{u}^{n+1} = \{\boldsymbol{U}_b^{n+1}\}$ and element pressures $\boldsymbol{p}^{n+1} = \{P_j^{n+1}\}$ (a total of $d \times n_{\text{node}} + n_{\text{elem}}$ unknowns). Given an approximation of the solution $(\boldsymbol{u}^{n+1,(k)}, \boldsymbol{p}^{n+1,(k)})$,

where (k) denotes the iteration level, Newton's method leads to the following system of Equations for the corrections:

$$\underbrace{\begin{bmatrix} \boldsymbol{K} & -\boldsymbol{L}^T \\ \boldsymbol{L} & \boldsymbol{F} \end{bmatrix}}_{\boldsymbol{J}} \begin{bmatrix} \delta\boldsymbol{u} \\ \delta\boldsymbol{p} \end{bmatrix}^{n+1,(k)} = - \begin{bmatrix} \boldsymbol{R}^u \\ \boldsymbol{R}^p \end{bmatrix}^{n+1,(k)}, \tag{28}$$

where $\boldsymbol{J}$ is the Jacobian matrix, $\boldsymbol{K}$ is the stiffness matrix, $\boldsymbol{L}$ is the coupling poromechanics matrix, and $\boldsymbol{F} = \boldsymbol{Q} + \Delta t \boldsymbol{T}$ is the flow matrix ($\boldsymbol{Q}$ is the compressibility matrix, and $\boldsymbol{T}$ the transmissibility matrix). The entries of the different matrices are:

$$\boldsymbol{K}_{ab} = \int_\Omega \boldsymbol{B}_a^T \boldsymbol{D} \boldsymbol{B}_b \, d\Omega, \tag{29}$$

$$\boldsymbol{L}_{ib} = \int_\Omega \varphi_i b (\mathbf{Grad}\, \eta_b)^T \, d\Omega, \tag{30}$$

$$Q_{ij} = \int_\Omega \varphi_i M^{-1} \varphi_j \, d\Omega, \tag{31}$$

and T_{ij} is the transmissibility between gridblocks i and j. The fully coupled method computes the Jacobian matrix $\boldsymbol{J}$, and determines $\delta\boldsymbol{u}$ and $\delta\boldsymbol{p}$ simultaneously, iterating until convergence.

Drained Split. In this scheme, the solution is obtained sequentially by first solving the mechanics problem, and then the flow problem. The pressure field is frozen when the mechanical problem is solved. The drained-split approximation of the operator $\mathcal{A}$ can be written as

$$\begin{bmatrix} \boldsymbol{u}^n \\ \boldsymbol{p}^n \end{bmatrix} \xrightarrow{\mathcal{A}^u_{dr}} \begin{bmatrix} \boldsymbol{u}^{n+1} \\ \boldsymbol{p}^n \end{bmatrix} \xrightarrow{\mathcal{A}^p_{dr}} \begin{bmatrix} \boldsymbol{u}^{n+1} \\ \boldsymbol{p}^{n+1} \end{bmatrix}, \quad \text{where} \quad \begin{cases} \mathcal{A}^u_{dr} : \mathrm{Div}\, \boldsymbol{\sigma} + \rho_b \boldsymbol{g} = \boldsymbol{0}, \, \delta p = 0, \\ \mathcal{A}^p_{dr} : \dot{m} + \mathrm{Div}\, \boldsymbol{q} = \rho_{f,0} f, \; \dot{\boldsymbol{\varepsilon}} : determined. \end{cases} \tag{32}$$

One solves the mechanical problem with no pressure change, then the fluid flow problem is solved with a frozen displacement field. We write the drained split as

$$\begin{bmatrix} \boldsymbol{K} & -\boldsymbol{L}^T \\ \boldsymbol{L} & \boldsymbol{F} \end{bmatrix} \begin{bmatrix} \delta\boldsymbol{u} \\ \delta\boldsymbol{p} \end{bmatrix} = \begin{bmatrix} \boldsymbol{K} & \boldsymbol{0} \\ \boldsymbol{L} & \boldsymbol{F} \end{bmatrix} \begin{bmatrix} \delta\boldsymbol{u} \\ \delta\boldsymbol{p} \end{bmatrix} - \begin{bmatrix} \boldsymbol{0} & \boldsymbol{L}^T \\ \boldsymbol{0} & \boldsymbol{0} \end{bmatrix} \begin{bmatrix} \delta\boldsymbol{u} \\ \delta\boldsymbol{p} \end{bmatrix}. \tag{33}$$

where we have dropped the explicit reference to the time step $n+1$ and iteration (k). In the drained split ($\delta\boldsymbol{p} = \boldsymbol{0}$), we solve the mechanics problem first as $\boldsymbol{K}\delta\boldsymbol{u} = -\boldsymbol{R}^u$. Then, the flow problem is solved as $\boldsymbol{F}\delta\boldsymbol{p} = -\boldsymbol{R}^p - \boldsymbol{L}\delta\boldsymbol{u}$. In this scheme, the fluid is allowed to flow when the mechanical problem is solved.

Undrained Split. In contrast to the drained method, the undrained split uses a different pressure predictor for the mechanical problem, which is computed by imposing that the fluid mass in each grid block remain constant during the mechanical step ($\delta m = 0$). The original operator $\mathcal{A}$ is split as follows:

$$\begin{bmatrix} \boldsymbol{u}^n \\ \boldsymbol{p}^n \end{bmatrix} \xrightarrow{\mathcal{A}^u_{ud}} \begin{bmatrix} \boldsymbol{u}^{n+1} \\ \boldsymbol{p}^{n+\frac{1}{2}} \end{bmatrix} \xrightarrow{\mathcal{A}^p_{ud}} \begin{bmatrix} \boldsymbol{u}^{n+1} \\ \boldsymbol{p}^{n+1} \end{bmatrix}, \quad \text{where} \quad \begin{cases} \mathcal{A}^u_{ud} : \mathrm{Div}\, \boldsymbol{\sigma} + \rho_b \boldsymbol{g} = \boldsymbol{0}, , \; \delta m = 0, \\ \mathcal{A}^p_{ud} : \dot{m} + \mathrm{Div}\, \boldsymbol{q} = \rho_{f,0} f, \; \dot{\boldsymbol{\varepsilon}} : determined. \end{cases} \tag{34}$$

The undrained strategy allows the pressure to change locally when the mechanical problem is solved. From Equation 3, the undrained condition ($\delta m = 0$) yields

$$0 = b\delta\varepsilon_v + \frac{1}{M}\delta p, \tag{35}$$

and the pressure is updated locally in each element using

$$p^{n+\frac{1}{2}} = p^n - bM(\varepsilon_v^{n+\frac{1}{2}} - \varepsilon_v^n). \tag{36}$$

For the mechanical problem, Equation 2 is discretized as follows:

$$\boldsymbol{\sigma}^{n+\frac{1}{2}} - \boldsymbol{\sigma}_0 = \mathbf{C}_{dr} : \boldsymbol{\varepsilon}^{n+\frac{1}{2}} - b(p^{n+\frac{1}{2}} - p_0)\mathbf{1}. \tag{37}$$

After substituting Equation 36 in Equation 37, the mechanical problem can be expressed in terms of displacements using the undrained bulk modulus, $\mathbf{C}_{ud} = \mathbf{C}_{dr} + b^2 M \mathbf{1} \otimes \mathbf{1}$. We write the undrained split as follows:

$$\begin{bmatrix} \boldsymbol{K} & -\boldsymbol{L}^T \\ \boldsymbol{L} & \boldsymbol{F} \end{bmatrix} \begin{bmatrix} \delta\boldsymbol{u} \\ \delta\boldsymbol{p} \end{bmatrix} = \begin{bmatrix} \boldsymbol{K} + \boldsymbol{L}^T\boldsymbol{Q}^{-1}\boldsymbol{L} & \boldsymbol{0} \\ \boldsymbol{L} & \boldsymbol{F} \end{bmatrix} \begin{bmatrix} \delta\boldsymbol{u} \\ \delta\boldsymbol{p} \end{bmatrix} - \begin{bmatrix} \boldsymbol{L}^T\boldsymbol{Q}^{-1}\boldsymbol{L} & \boldsymbol{L}^T \\ \boldsymbol{0} & \boldsymbol{0} \end{bmatrix} \begin{bmatrix} \delta\boldsymbol{u} \\ \delta\boldsymbol{p} \end{bmatrix}. \tag{38}$$

Note that the undrained condition is written as $\boldsymbol{Q}\delta\boldsymbol{p} + \boldsymbol{L}\delta\boldsymbol{u} = \boldsymbol{0}$. This implies $(\boldsymbol{K} + \boldsymbol{L}^T\boldsymbol{Q}^{-1}\boldsymbol{L})\delta\boldsymbol{u} = -\boldsymbol{R}^u$ during the mechanical step. The matrix multiplication for calculating $\boldsymbol{L}^T\boldsymbol{Q}^{-1}\boldsymbol{L}$ is not required, since this calculation simply entails using the undrained moduli. Then, the fluid flow problem is solved, with $\boldsymbol{F}\delta\boldsymbol{p} = -\boldsymbol{R}^p - \boldsymbol{L}\delta\boldsymbol{u}$. The additional computational cost is negligible because the calculation of $\boldsymbol{p}^{n+1/2}$ is explicit.

Fixed-strain Split. In this scheme, the flow problem is solved first. The original operator $\mathcal{A}$ is approximated and split in the following manner.

$$\begin{bmatrix}\boldsymbol{u}^n\\ \boldsymbol{p}^n\end{bmatrix} \xrightarrow{\mathcal{A}^p_{sn}} \begin{bmatrix}\boldsymbol{u}^{n+\frac{1}{2}}\\ \boldsymbol{p}^{n+1}\end{bmatrix} \xrightarrow{\mathcal{A}^u_{sn}} \begin{bmatrix}\boldsymbol{u}^{n+1}\\ \boldsymbol{p}^{n+1}\end{bmatrix}, \quad \text{where} \quad \begin{cases}\mathcal{A}^p_{sn} : \dot{m} + \operatorname{Div}\boldsymbol{q} = \rho_{f,0} f,\ \delta\dot{\varepsilon}_v = 0,\\ \mathcal{A}^u_{sn} : \operatorname{Div}\boldsymbol{\sigma} + \rho_b \boldsymbol{g} = \boldsymbol{0},\ p : determined.\end{cases} \tag{39}$$

From the fixed-strain split, $\delta\dot{\varepsilon}_v = 0$, which implies that $\dot{\varepsilon}_v^{n+1/2} = \dot{\varepsilon}_v^n$, so the volumetric strain term $b\dot{\varepsilon}_v$ in the accumulation term of Equation 11 for the flow problem is computed explicitly. We write the fixed-strain split as follows:

$$\begin{bmatrix}\boldsymbol{K} & -\boldsymbol{L}^T\\ \boldsymbol{L} & \boldsymbol{F}\end{bmatrix}\begin{bmatrix}\delta\boldsymbol{u}\\ \delta\boldsymbol{p}\end{bmatrix} = \begin{bmatrix}\boldsymbol{K} & -\boldsymbol{L}^T\\ \boldsymbol{0} & \boldsymbol{F}\end{bmatrix}\begin{bmatrix}\delta\boldsymbol{u}\\ \delta\boldsymbol{p}\end{bmatrix} - \begin{bmatrix}\boldsymbol{0} & \boldsymbol{0}\\ -\boldsymbol{L} & \boldsymbol{0}\end{bmatrix}\begin{bmatrix}\delta\boldsymbol{u}\\ \delta\boldsymbol{p}\end{bmatrix}. \tag{40}$$

We first solve the flow problem $\boldsymbol{F}\delta\boldsymbol{p} = -\boldsymbol{R}^p$ while freezing the strain field (i.e. $\delta\dot{\boldsymbol{\varepsilon}} = \boldsymbol{0}$, or equivalently $-\boldsymbol{L}\delta\boldsymbol{u} = \boldsymbol{0}$). Then, we solve the mechanical problem as $\boldsymbol{K}\delta\boldsymbol{u} = -\boldsymbol{R}^u + \boldsymbol{L}^T\delta\boldsymbol{p}$. It is worth noting that the mechanical problem uses the drained rock properties, and that the pressure corrections act as "loads" (Settari and Mourits, 1998).

Fixed-stress Split. In this case, the flow problem is solved first, but now freezing the total mean stress field ($\delta\dot{\sigma}_v = 0 \Rightarrow \dot{\sigma}_v^{n+1/2} = \dot{\sigma}_v^n$), so the volumetric stress term $(b/K_{dr})\dot{\sigma}_v$ in the accumulation term of Equation 13 for the flow problem is computed explicitly.

The original operator $\mathcal{A}$ is decomposed as follows:

$$\begin{bmatrix}\boldsymbol{u}^n\\ \boldsymbol{p}^n\end{bmatrix} \xrightarrow{\mathcal{A}^p_{ss}} \begin{bmatrix}\boldsymbol{u}^{n+\frac{1}{2}}\\ \boldsymbol{p}^{n+1}\end{bmatrix} \xrightarrow{\mathcal{A}^u_{ss}} \begin{bmatrix}\boldsymbol{u}^{n+1}\\ \boldsymbol{p}^{n+1}\end{bmatrix}, \quad \text{where} \quad \begin{cases}\mathcal{A}^p_{ss} : \dot{m} + \operatorname{Div}\boldsymbol{q} = \rho_{f,0} f,\ \delta\dot{\sigma}_v = 0,\\ \mathcal{A}^u_{ss} : \operatorname{Div}\boldsymbol{\sigma} + \rho_b \boldsymbol{g} = \boldsymbol{0},\ p : determined.\end{cases} \tag{41}$$

If we fixed the rate of the entire stress tensor field during the solution of the flow problem, the condition to be satisfied is $-\boldsymbol{L}\delta\boldsymbol{u} + \boldsymbol{L}\boldsymbol{K}^{-1}\boldsymbol{L}^T\delta\boldsymbol{p} = \boldsymbol{0}$. We write the fixed-stress split as

$$\begin{bmatrix}\boldsymbol{K} & -\boldsymbol{L}^T\\ \boldsymbol{L} & \boldsymbol{F}\end{bmatrix}\begin{bmatrix}\delta\boldsymbol{u}\\ \delta\boldsymbol{p}\end{bmatrix} = \begin{bmatrix}\boldsymbol{K} & -\boldsymbol{L}^T\\ \boldsymbol{0} & \boldsymbol{F} + \boldsymbol{L}\boldsymbol{K}^{-1}\boldsymbol{L}^T\end{bmatrix}\begin{bmatrix}\delta\boldsymbol{u}\\ \delta\boldsymbol{p}\end{bmatrix} - \begin{bmatrix}\boldsymbol{0} & \boldsymbol{0}\\ -\boldsymbol{L} & \boldsymbol{L}\boldsymbol{K}^{-1}\boldsymbol{L}^T\end{bmatrix}\begin{bmatrix}\delta\boldsymbol{u}\\ \delta\boldsymbol{p}\end{bmatrix}. \tag{42}$$

Thus, in the fixed-stress split, we first solve the flow problem with $(\boldsymbol{F} + \boldsymbol{L}\boldsymbol{K}^{-1}\boldsymbol{L}^T)\delta\boldsymbol{p} = -\boldsymbol{R}^p$. In the fixed *mean*-stress split, however, the full matrix inversion and multiplication $\boldsymbol{L}\boldsymbol{K}^{-1}\boldsymbol{L}^T$ is not required, since the rate of mean stress is kept constant by introducing the term b^2/K_{dr} locally in each element (see Equation 13). Once the flow problem is solved, we solve the mechanical problem exactly as for the fixed-strain split.

Fixed-strain and Fixed-stress Methods vs. the Pore Compressibility Approach. In traditional reservoir simulation, the pressure equation typically employs a 'pore compressibility', c_p, expressed as

$$(\phi_0 c_f + \phi_0 c_p)\frac{\partial p}{\partial t} + \operatorname{Div}\boldsymbol{v} = f. \tag{43}$$

The pore compressibility is not an intrinsic parameter of the rock, since it depends on the deformation scenario and the boundary conditions of the coupled problem. It is used in traditional reservoir simulation as a simplified way to account for changes in the state of stress and strain in the reservoir (Settari and Mourits, 1998; Settari and Walters, 2001). From Equations 5, 11, and 43, the fixed-strain split takes $\phi_0 c_p|_{sn}$ as $(b-\phi_0)/K_s$, and $b\dot{\varepsilon}_v$ as a correction source term due to mechanical effects. Similarly, from Equations 5, 13, and 43, the fixed-stress split takes $\phi_0 c_p|_{ss} = (b-\phi_0)/K_s + b^2/K_{dr}$, and $b/K_{dr}\dot{\sigma}_v$ as a correction source term from the mechanical solution. The expression for the pore compressibility associated with the fixed-stress split coincides with the one proposed by Settari and Mourits (1998) (albeit for linear poroelasticity only). Other values of c_p can be used in order to enhance the stability and convergence of a sequential-implicit scheme. This possibility has been studied, in the context of linear poroelasticity, by Bevillon and Masson (2000), and Mainguy and Longuemare (2002).

In order to properly account for geomechanical effects, a correction needs to be included as a source term. This source term is known as *porosity correction*, $\Delta\Phi$ (Mainguy and Longuemare, 2002) and takes the following two equivalent expressions:

$$\Delta\Phi = \left(\phi_0 c_p + \frac{\phi_0 - b}{K_s}\right)\dot{p} - b\dot{\varepsilon}_v \qquad \text{(from Equation 11)}, \tag{44}$$

$$= \left(\phi_0 c_p + \frac{\phi_0}{K_s} - \frac{b}{K_{dr}}\right)\dot{p} - \left(\frac{1}{K_{dr}} - \frac{1}{K_s}\right)\dot{\sigma}_v \qquad \text{(from Equation 13)}. \tag{45}$$

Even though the 'pore compressibility' has been recognized as a stabilization term, a complete stability analysis and comparison study of sequential methods including plasticity is lacking. In the next section, we analyze the stability and accuracy of the four sequential methods presented here.

Stability Analysis for Linear Poroelasticity

Von Neumann Stability Analysis. We use the Von Neumann method to analyze the stability of sequential-implicit coupling strategies. This method is frequently used to analyze the stability of linear, or linearized, problems with respect to time (see, e.g. Strikwerda (2004); Miga et al. (1998); Wan et al. (2005)). The details of the stability analysis are given elsewhere (Kim, 2009). Here, we simply report the expressions (either explicit or quadratic equations) of the amplification factors γ for one-dimensional problems:

$$\text{Fully coupled :} \quad \gamma_{fc} = \begin{cases} 0, \\ \dfrac{\frac{K_{dr}}{M} + b^2}{\frac{K_{dr}}{M} + b^2 + K_{dr}\frac{k\Delta t}{\mu}\frac{1}{h^2}2(1-\cos\theta)} \leq 1, \end{cases} \tag{46}$$

$$\text{Drained split :} \quad \left[\frac{K_{dr}}{M} + K_{dr}\frac{k\Delta t}{\mu}\frac{1}{h^2}2(1-\cos\theta)\right]\gamma_{dr}^2 - \left[\frac{K_{dr}}{M} - b^2\right]\gamma_{dr} - b^2 = 0, \tag{47}$$

$$\text{Undrained split :} \quad \gamma_{ud} = \begin{cases} 0, \\ \dfrac{\frac{K_{dr}+b^2M}{M} + \frac{b^2Mk\Delta t}{\mu}\frac{1}{h^2}2(1-\cos\theta)}{\frac{K_{dr}+b^2M}{M} + \frac{(K_{dr}+b^2M)k\Delta t}{\mu}\frac{1}{h^2}2(1-\cos\theta)} \leq 1, \end{cases} \tag{48}$$

$$\text{Fixed-strain split :} \quad \left[\frac{K_{dr}}{M} + K_{dr}\frac{k\Delta t}{\mu}\frac{1}{h^2}2(1-\cos\theta)\right]\gamma_{sn}^2 - \left[\frac{K_{dr}}{M} - b^2\right]\gamma_{sn} - b^2 = 0, \tag{49}$$

$$\text{Fixed-stress split :} \quad \gamma_{ss} = \begin{cases} 0, \\ \dfrac{\frac{K_{dr}}{M} + b^2}{\frac{K_{dr}}{M} + b^2 + K_{dr}\frac{k\Delta t}{\mu}\frac{1}{h^2}2(1-\cos\theta)} \leq 1. \end{cases} \tag{50}$$

In these expressions, Δt and h are the timestep size and spatial grid spacing, respectively, and θ is the phase parameter in the Von Neumann method.

The amplification factors are less than one and non-negative for the fully coupled (γ_{fc}), undrained (γ_{ud}), and fixed-stress (γ_{ss}) schemes; as a result, unconditional stability and non-oscillatory solutions as a function of time are expected for these methods. Note that the amplification factors of the fixed-stress split (Eq.50) and the fully coupled scheme (Eq.50) are identical. Numerical simulations, which are discussed later, confirm that the fixed-stress split enjoys excellent stability and convergence properties.

Equations 47 and 49 indicate that the amplification factors of the drained and fixed-strain splits are the same. Therefore, the drained and fixed-strain methods are conditionally stable, and they share the same stability limit, namely,

$$\tau = \frac{b^2M}{K_{dr}} \leq 1, \tag{51}$$

where τ is referred to as the *coupling strength*, and it is given by the ratio of the bulk stiffness of the fluid and solid skeleton. The stability results can be extended from one to multiple dimensions, since the coupling between flow and mechanics is due to the volumetric response, which is a scalar quantity. In one dimension, K_{dr} is the constrained modulus; in the two dimensional plane-strain case, K_{dr} is $\frac{1}{4}\mathbf{1}_2^T\boldsymbol{D}_{ps}\mathbf{1}_2$; in three dimensions, K_{dr} is the drained bulk modulus, which is given by $\frac{1}{9}\mathbf{1}_3^T\boldsymbol{D}_{dr}\mathbf{1}_3$, where $\mathbf{1}_2^T = [1,1,0]$, $\mathbf{1}_3^T = [1,1,1,0,0,0]$, $\boldsymbol{D}_{ps}$ is a 3×3 matrix given by Equation 24, and $\boldsymbol{D}_{dr}$ is a 6×6 matrix involving the drained moduli (Hughes, 1987). The coupling strength can be extended to multi-dimensional, elasto-plasticity as follows:

$$\tau = \frac{b^2M}{\frac{1}{9}\mathbf{1}_3^T\boldsymbol{D}_{ep}\mathbf{1}_3}, \tag{52}$$

where $\boldsymbol{D}_{ep}$ is the elasto-plastic tangent modulus (in compact engineering notation) in three dimensions.

It is important to note the drained and fixed-strain methods have negative amplification factors, which implies the possibility of oscillatory numerical behavior as a function of time, even when the stability limit is honored. This is indeed confirmed by numerical solutions (Kim, 2009).

In reservoir engineering applications, the fluid system (usually oil and water) is assumed to be (at minimum) slightly compressible. Nevertheless, it is important to understand the stability characteristics of coupled flow-mechanics problems in the limit of incompressible fluids. When both the fluid and solid (the grains that makes up the rock) are incompressible, the Biot modulus, M, is infinite. As a result, the coupling strength, τ, as defined here is infinite. In this case, the fixed-stress split has $max(|\gamma|) < 1$ indicating stability. In contrast, the undrained split in this case has distinct amplification factors with $max(|\gamma|) = 1$, which indicates bounded error propagation (stability) but with expected convergence difficulties (Kim, 2009). Note that in this (incompressible) limit case, both the drained and fixed-strain methods are unconditionally unstable.

Numerical Simulations. Numerical solutions of simple 1D problems confirm that the undrained and fixed-stress methods are unconditionally stable and convergent (Kim, 2009). These 1D solutions also confirm that the stability criteria for the drained and fixed-strain splits are valid and sharp. That is, small violations of the stability limit lead to unstable solutions. Moreover, consistent with Equation 51, the numerical solutions confirm that the drained and fixed-strain stability limit depends on the coupling strength only and is independent of the time step size. The details of these simple 1D test cases are given elsewhere(Kim, 2009).

Below, we describe the results from numerical simulations of three test cases.

Case 1 Injection and production in a 1D poroelastic medium. The driving force is due to injection and production (Figure 2). The focus is on the behaviors as function of coupling strength. Dilation and compaction take place around the injection and production wells, respectively.

Case 2 Mandel's problem in a 2D elastic medium. The driving force is provided by the side-burden (the left picture in Figure 3).

Case 3 Fluid production scenario in 2D with elasto-plastic behavior described by the modified Cam-clay model. Compaction of the reservoir occurs due to production (the right diagram in Figure 3). Plasticity leads to significant compaction.

Next, the results for the first two cases, which assume linear poroelastic behavior, are presented. The results are based on *one iteration* per time step (i.e., solve one problem implicitly, then solve the other problem implicitly), unless noted explicitly otherwise.

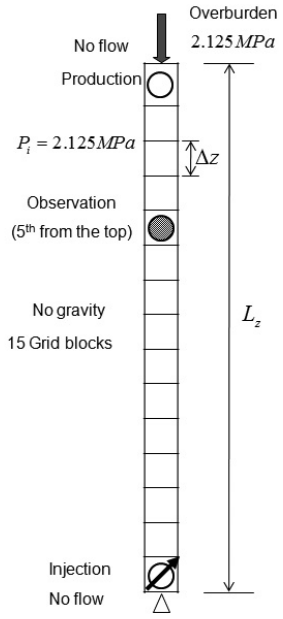

Figure 2: 1D problem with injection and production wells (Case 1).

Table 1: Input data for Case 1

Property	Value
Permeability (k)	50 md
Porosity (ϕ_0)	0.3
Constrained modulus (K_{dr})	100 MPa
Biot coefficient (b)	1.0
Bulk density (ρ_b)	2400 kg m^{-3}
Fluid density ($\rho_{f,0}$)	1000 kg m^{-3}
Fluid viscosity (μ)	1.0 cp
Injection rate (Q_{inj})	100 kg day^{-1}
Production rate (Q_{prod})	100 kg day^{-1}
Boundary pressure ($\bar{p}$)	2.125 MPa
Overburden ($\bar{\sigma}$)	2.125 MPa
Grid spacing (Δz)	10 m

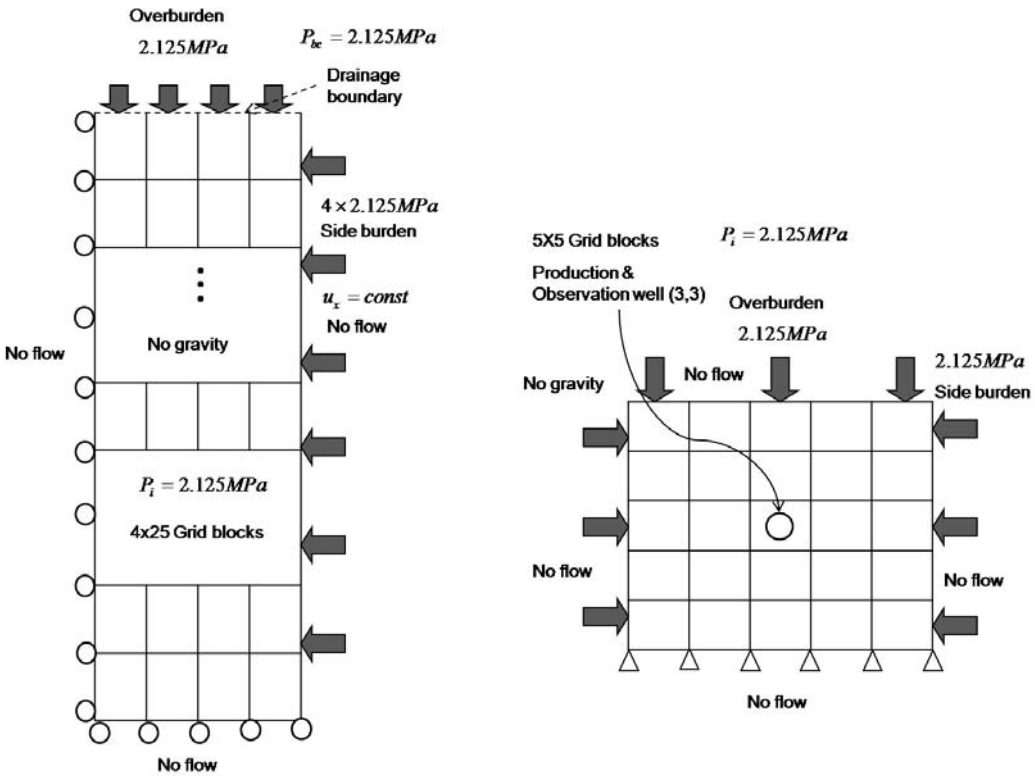

Figure 3: Left: Mandel's problem in 2D with elastic deformation (Case 2). Right: 2D problem driven by single-well production in an elastoplastic medium (Case 3).

Case 1 The numerical values of the parameters for Case 1 are given in Table 1. Here $b = 1.0$ (i.e., incompressible solid grains, $K_s = \infty$). Given the coupling strength τ, $M = \tau K_{dr}/b^2$. Figure 4 shows a comparison between the undrained and fixed-stress schemes for Case 1, at high coupling strength. As shown in the figure, the fixed-stress scheme converges after one iteration per time step. This behavior is consistent with the fact that the amplification factors of the fully coupled and fixed-stress split methods are identical. On the other hand, several iterations are required in order for the undrained method to match (within a very small tolerance) the fully coupled solution. For this linear coupled problem, the fixed-stress split takes two iterations to match the fully coupled solution when the exact K_{dr} is used (Kim, 2009). In problems with more complex boundary conditions, estimating K_{dr} can be quite difficult and is, in fact, part of the problem. In such problems, the fixed-stress scheme may require several iterations to converge.

Case 2 – Mandel's Problem. Mandel's problem is commonly used to show the validity of simulators for coupled flow and geomechanics. A description and analytical solution of Mandel's problem is presented in Abousleiman et al. (1996). The input parameters are listed in Table 2. Figure 5 shows that the drained method (left figure) is stable when τ is less than one, while it is unstable when τ is greater than one. Furthermore, severe oscillations are observed even though the drained split is stable. Due to the oscillations, the early time solution is not computed properly in the drained split even though the late time solution converges to the analytical results. On the other hand, the undrained method shows unconditional stability and yields a monotonic solution that matches the analytical solution at all times. Figure 6 indicates that the fixed-strain split (left figure) is stable for $\tau < 1$, while it is unstable when $\tau > 1$. Similarly to the drained split method, the fixed-strain split method can yield severe oscillations at early time. The fixed-stress split, on the other hand, is stable and non-oscillatory under all conditions.

The *Mandel–Cryer effect*, where a rise in the pressure during early time is observed, can be captured by properly constructed sequential methods. All solutions from the fully coupled, undrained, and fixed-stress methods are in good agreement with the analytical solution.

Stability Analysis: Nonlinear Poro-elastoplasticity

Coupling with Elastoplasticity. The coupling between the mechanical and the flow problems in the elastoplastic regime under isothermal conditions is modeled by the following constitutive equations (Coussy, 1995):

$$\boldsymbol{\sigma} - \boldsymbol{\sigma}_0 = \mathbf{C}_{dr} : (\boldsymbol{\varepsilon} - \boldsymbol{\varepsilon}_p) - b(p - p_0)\mathbf{1}, \tag{53}$$

$$\frac{1}{\rho_{f,0}}(m - m_0) - \phi_p = b(\varepsilon_v - \varepsilon_{p,v}) + \frac{1}{M}(p - p_0), \tag{54}$$

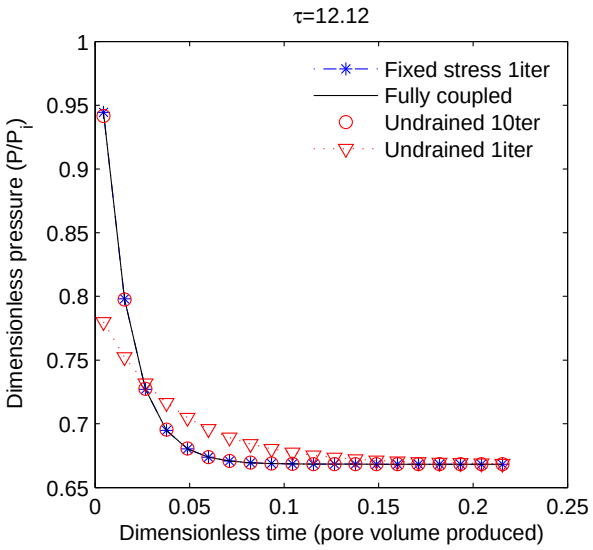

Figure 4: Behavior of the undrained and fixed-stress splits for cases with very high coupling strength. Case 1 with $\tau = 12.12$. The fixed-stress method requires one single iteration per time step to match the fully coupled solution, while many more iterations are required for the undrained method.

Table 2: Input data for Case 2

Property	Value
Permeability (k)	50 md
Porosity (ϕ_0)	0.3
Young modulus (E)	2900 MPa
Poisson ratio (ν)	0
Biot coefficient (b)	1.0
Bulk density (ρ_b)	2400 kg m^{-3}
Fluid density ($\rho_{f,0}$)	1000 kg m^{-3}
Fluid viscosity (μ)	1.0 cp
Initial pressure (p_i)	2.125 MPa
Boundary pressure ($\bar{p}$)	2.125 MPa
Side burden	4×2.125 MPa
Overburden ($\bar{\sigma}$)	2.125 MPa
Grid spacing (Δx)	0.005 m
Grid spacing (Δz)	2.0 m
Grid	4×25

where $\boldsymbol{\varepsilon}_p$ is the linearized plastic strain tensor due to inelasticity, $\varepsilon_{p,v} = \mathrm{tr}\boldsymbol{\varepsilon}_p$, and ϕ_p is the plastic porosity. The plastic porosity and plastic strain can be related to each other by assuming that $\dot{\phi}_p = \beta\dot{\varepsilon}_{p,v}$. Here, we assume that $\beta = b$ (Armero, 1999). Note that $\beta \approx b \approx 1$ if the solid grains are incompressible. The relation between the total stress $\boldsymbol{\sigma}$ and total strain $\boldsymbol{\varepsilon}$ is written as

$$\boldsymbol{\sigma} - \boldsymbol{\sigma}_0 = \mathbf{C}_{dr} : (\boldsymbol{\varepsilon} - \boldsymbol{\varepsilon}_p) - b(p - p_0)\mathbf{1} = \mathbf{C}_{ep} : \boldsymbol{\varepsilon} - b(p - p_0)\mathbf{1}, \tag{55}$$

where $\mathbf{C}_{ep}$ is the rank-4 elastoplastic tangent tensor. The compact engineering notation for $\mathbf{C}_{ep}$ and $\mathbf{1}$ are $\boldsymbol{D}_{ep}$ and $\mathbf{1}_3^T$, respectively (this notation is employed in Equation 52). Elastoplasticity renders the mechanical problem highly nonlinear.

Stability analysis of slightly compressible flow and nonlinear mechanical deformation can be performed using the Von Neumann method through linearization of the problem. The difference with respect to the linear problem is that the coefficients of the stability conditions, such as $\boldsymbol{D}_{ep}$ and K_{dr}, are linearized around values from the previous iteration (using Newton's method), for example.

Our analysis of the linearized systems shows that the fully coupled, undrained, and fixed-stress methods yield unconditional stability regardless of $\boldsymbol{D}_{ep}$ and K_{dr}. However, the drained and fixed-strain methods show strong dependency on the coupling strength defined in Equation 52. This implies that the drained and fixed-strain methods can be unstable as the medium begins to yield (plastic regime), even if they satisfy the stability conditions at the beginning of a simulation (elastic regime).

For nonlinear problems, one can apply a sequential solution method before, or after linearization. In this paper, we are interested in sequential implicit-implicit schemes, where each iteration involves solving two problems in sequence, such that

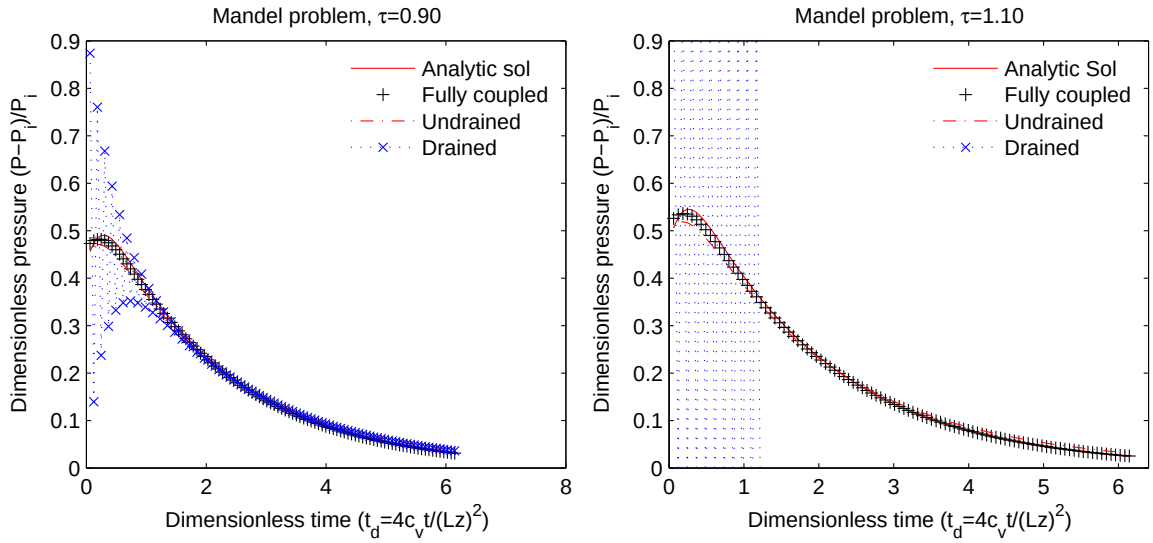

Figure 5: Case 2 (Mandel's problem). Evolution of the pressure at the observation point, as a function of dimensionless time. The results of the fully coupled, drained, and undrained methods are shown for two values of the coupling strength. Left: $\tau = 0.90$**. Right:** $\tau = 1.10$**.** $\Delta t_d = \frac{4c_v \Delta t}{(L_z)^2}$**, where** c_v **is the consolidation coefficient defined as** $c_v = \frac{k}{(1/K_{dr}+\phi c_f)\mu}$**.** L_z **is the vertical length of the reservoir domain**

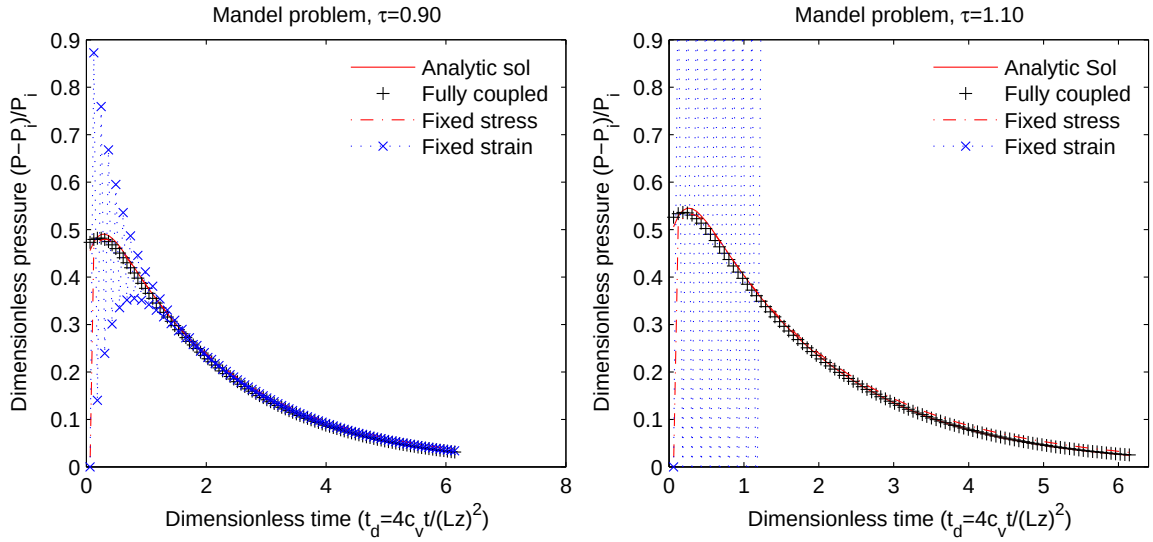

Figure 6: Case 2 (Mandel's problem). Evolution of the pressure at the observation point, as a function of dimensionless time. Shown are the results for the fully coupled, fixed-strain, and fixed-stress splits. Left: $\tau = 0.90$**. Right:** $\tau = 1.10$**.**

each problem, which may be nonlinear, is solved implicitly. For a given timestep, a single-pass strategy would entail solving the first sub-problem implicitly (subject to a given tolerance), updating the appropriate terms to set up the second problem, and solving the second problem implicitly. We then move to the next time step. One can also iterate by repeating the implicit-implicit solution sequence.

Numerical Simulations. To test the validity of the results obtained from our linearized stability analysis, we perform numerical experiments for Case 3. We adopt an associated plasticity formulation (Simo, 1991; Simo and Hughes, 1998; Coussy, 1995). The yield function f_Y of the modified Cam-clay model is (Borja and Lee, 1990)

$$f_Y = \frac{q'^2}{M_{\text{mcc}}^2} + \sigma'_v(\sigma'_v - p_{co}) = 0, \tag{56}$$

where q' is the deviatoric effective stress, σ'_v is the volumetric effective stress, M_{mcc} is the slope of the critical state line, and p_{co} is the preconsolidation pressure. The input parameters for Case 3 are listed in Table 3. The parameter λ is the virgin compression index, and κ is the swell index. The schematic of the return mapping for the modified Cam-clay model is illustrated

in Figure 7 (refer to Borja and Lee (1990) for more details). We employ full iteration with a consistent return-mapping algorithm (Simo and Hughes, 1998).

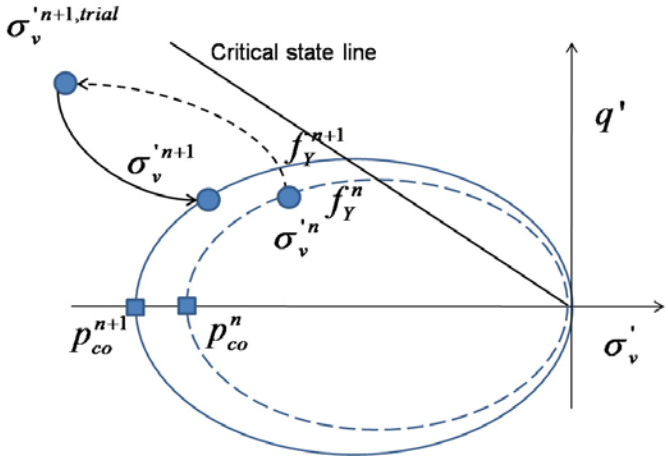

Figure 7: schematic of the return mapping algorithm for the modified Cam-clay model.

Table 3: Input data for Case 3

Property	Value
Permeability (k)	50 md
Porosity (ϕ_0)	0.3
Young modulus (E)	350 MPa
Poisson ratio (ν)	0.35
Biot coefficient (b)	1.0
Bulk density (ρ_b)	2400 kg m^{-3}
Fluid density ($\rho_{f,0}$)	1000 kg m^{-3}
Fluid viscosity (μ)	1.0 cp
Virgin compression index (λ)	0.37
Swell index (κ)	0.054
Critical state slope (M_{mcc})	1.4
Preconsolidation pressure ($p_{co,0}$)	-1.0 MPa
Initial pressure (p_0)	2.125 MPa
Sideburden ($\bar{\sigma}_h$)	2.125 MPa
Overburden ($\bar{\sigma}_v$)	2.125 MPa
Grid spacing (Δx)	10 m
Grid spacing (Δz)	10 m
Grid	5×5

Figure 8 shows that the drained and fixed-strain split methods are stable during the early-time elastic regime, which has a weak coupling strength ($\tau < 1$). However, when plasticity is reached, the solution by the drained method is no longer stable because the coupling strength increases dramatically. Figure 9 depicts the variation of the coupling strength during the simulation. It is clear that when the coupling strength increases beyond unity, the solution by the drained and fixed-strain methods becomes unstable. No solution by the drained and fixed-strain split methods is possible after plasticity. On the other hand, the fully coupled, undrained, and fixed-stress methods provide stable results well into the plastic regime, as shown in Figure 8. In particular, the solution of the fully coupled method is matched by the undrained and fixed-stress splits after only two iterations.

We also show the results using full Newton iterations (i.e., a sequential solution strategy is employed to solve the linear system of equations associated with each Newton iteration of the fully coupled system). Figure 10 shows that using such a strategy, the drained and fixed-strain splits are unstable as we enter the plastic regime, even though they are stable in the elastic regime. On the other hand, the undrained and fixed-stress splits are stable, even for plastic deformation.

Summary and Conclusions

We employed the Von Neumann method to analyze the stability properties of several sequential-implicit solution strategies for coupled flow and mechanical deformation in oil reservoirs. Detailed numerical simulations of several representative problems

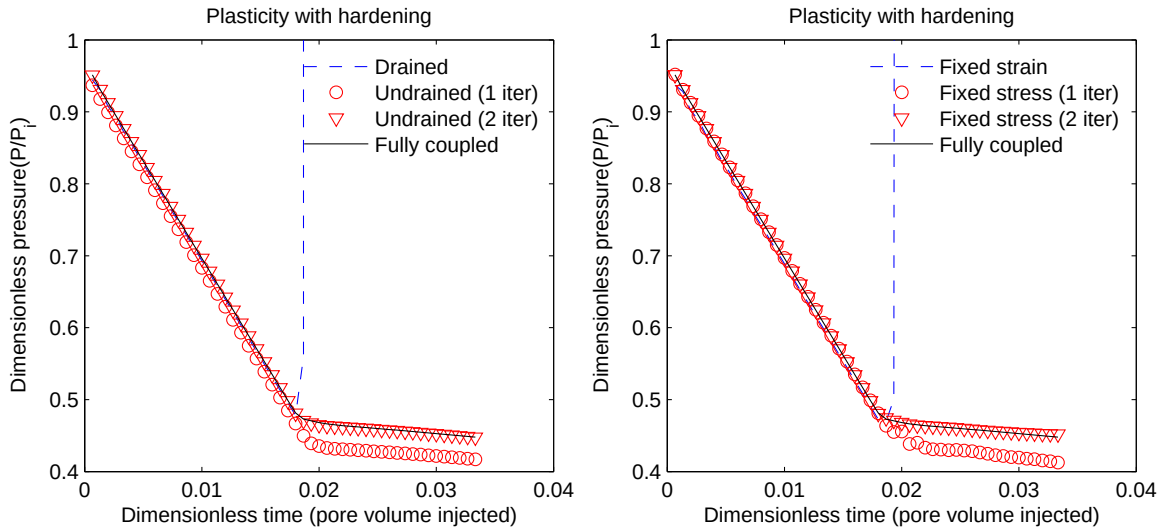

Figure 8: Case 3 (2D production test in the elastoplastic regime). Evolution of the dimensionless pressure at the observation point is shown as a function of dimensionless time (pore volumes produced). Left: fully coupled, drained, and undrained numerical solutions. Right: fully coupled, fixed-strain, and fixed-stress solutions. The undrained and fixed-stress splits yield stable solution, while the drained and fixed-strain splits become unstable as the problem enters the plastic regime.

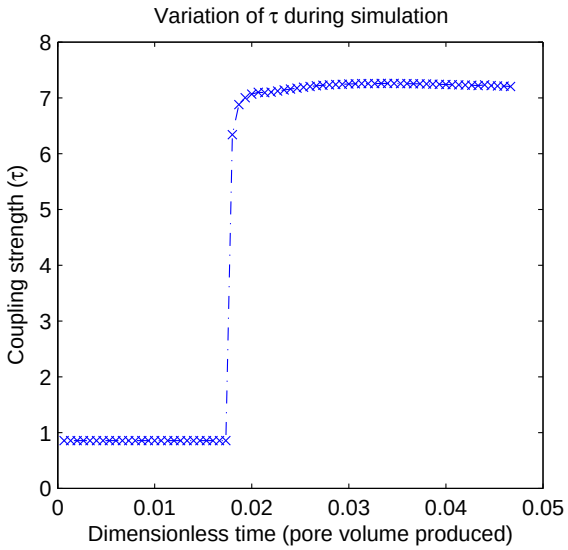

Figure 9: Variation of the coupling strength τ during the course of the simulation for Case 3. The coupling strength, initially less than one, jumps to a very high value when the medium enters the plastic regime, rendering the drained and fixed-strain methods unstable.

were used to test the validity of the stability analysis. The study is limited to single-phase flow of a slightly compressible fluid; however, both elastic and elasto-plastic material behaviors are investigated. The four sequential methods investigated fall in two categories: those that solve the mechanical problem first (drained and undrained splits), and those that solve the flow problem first (fixed-strain and fixed-stress splits).

The drained split, in which the pressure is frozen while solving the mechanics problem, and the fixed-strain split, in which the displacements are frozen while solving the flow problem, are the obvious sequential solution strategies. As we show quite clearly in this work, however, these two schemes suffer from severe stability and convergence problems. Specifically, the drained and fixed-strain split methods are conditionally stable; moreover, their stability limit ($\tau < 1$) depends on the coupling strength only and is independent of timestep size. Thus, physical problems with high coupling strength (i.e., $\tau > 1$) cannot be solved by the drained or fixed-strain split methods, regardless of the time step size. Even when they are stable, the drained and fixed-strain splits display oscillatory behavior, which is implied by their negative amplification factors.

In contrast, the undrained and fixed-stress methods show unconditional stability for both elasticity and elasto-plasticity. These sequential methods can be applied safely to model poro-mechanical problems of practical interest, such as compressible solid grains and plasticity with hardening. Moreover, in addition to the amplification factors being less than unity, they are

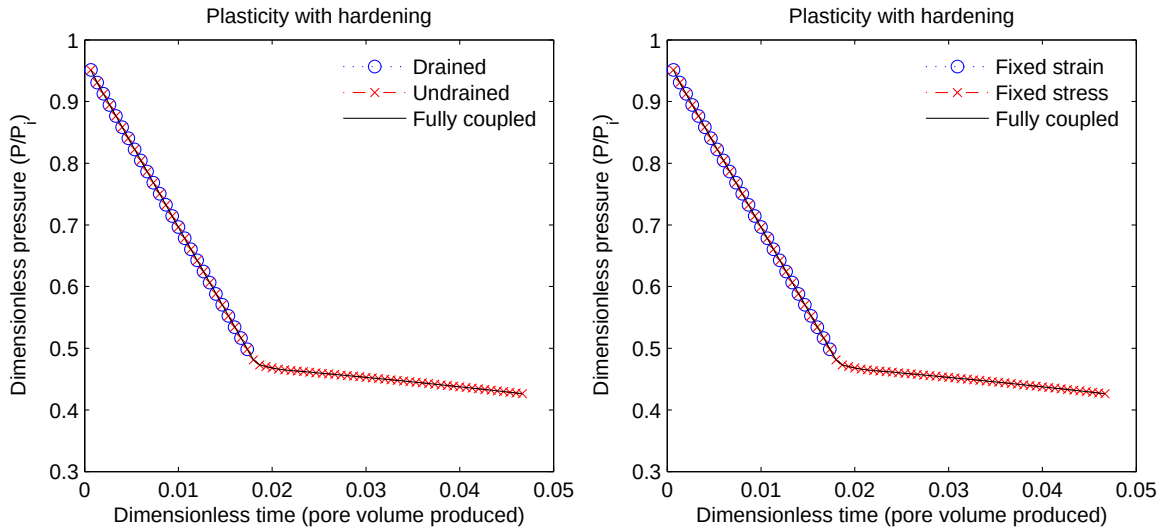

Figure 10: Case 4 (2D production test in elastoplastic regime). Shown is the evolution of the dimensionless pressure at the observation point against dimensionless time (pore volumes produced). Left: fully coupled, drained, and undrained numerical solutions. Right: fully coupled, fixed-strain, and fixed-stress solutions. The model enters the plastic regime at $t_d \approx 0.018$. Beyond this point, the drained and fixed-strain methods become unstable and fail to produce a solution at all.

positive; as a result, the numerical solutions do not exhibit oscillations in time.

While the undrained split and fixed-stress split have similar stability properties, we have found that for the problems we studied the fixed-stress scheme converges much faster than the undrained method. This behavior was observed across a wide range of the coupling strength. Based on these findings, we strongly recommend the fixed-stress split over the other sequential-implicit methods for modeling coupled geomechanics and flow in oil reservoirs.

Acknowledgements. This work was supported by Foundation CMG (Computer Modeling Group), the Stanford University Petroleum Research Institute for Reservoir Simulation (SUPRI-B), and the Reed Research Fund.

Nomenclature.

$\boldsymbol{B}_a$ Linearized strain operator

B_f Formation volume factor of the fluid

$\mathbf{C}_{dr}$ Rank-4 drained elasticity tensor

$\mathbf{C}_{ep}$ Rank-4 elastoplastic tangent tensor

$\mathbf{C}_{ud}$ Rank-4 undrained elasticity tensor

$\boldsymbol{D}_{ps}$ Elasticity matrix for the plane strain case in 2D

$\boldsymbol{D}_{dr}$ Drained modulus matrix (compact engineering notation for $\mathbf{C}_{dr}$) in 3D

$\boldsymbol{D}_{ep}$ Elastoplastic tangent modulus matrix (compact engineering notation for $\mathbf{C}_{ep}$) in 3D

$\mathrm{Div}(\cdot)$ Divergence operator

E Young's modulus

$\boldsymbol{F}$ Flow matrix

$\boldsymbol{J}$ Jacobian matrix

$\boldsymbol{K}$ Stiffness matrix

K_{dr} Drained bulk modulus used for the definition of the coupling strength

K_f Bulk modulus of the fluid

K_s Bulk modulus of the solid grain

$\boldsymbol{L}$ Coupling poromechanics matrix

M Biot's modulus

$M_{\mathbf{mcc}}$ Slope of the critical state line of the modified Cam-clay model

P_j Pressure at the element j

$\boldsymbol{Q}$ Compressibility matrix

$Q_{\mathbf{inj}}$ Injection rate

$Q_{\mathbf{prod}}$ Production rate

$\boldsymbol{R}_a^u$, R_j^p Residuals for mechanics (node a) and flow (element j)

$\boldsymbol{T}$ Transmissibility matrix

T_{ij} Transmissibility between gridblocks i and j

$\boldsymbol{U}_b$ Displacement vector at the node b

$V_{h,ij}$ Flux between gridblocks i and j

b Biot's coefficient

c_f Fluid compressibility ($1/K_f$)

c_p Pore compressibility

c_v Consolidation coefficient

$\boldsymbol{e}$ Deviatoric part of the strain tensor

$\|\mathbf{e}_{P_d}\|$ L_2 norm of the error for the dimensionless pressure

f Volumetric source term for flow

f_Y Yield function for elastoplasticity

$\boldsymbol{g}$ Gravity vector

h Grid spacing used in the Von Neumann method

$\boldsymbol{k}$ Absolute permeability tensor

m Fluid mass per unit bulk volume

$n_{\mathbf{elem}}$ Number of elements

$n_{\mathbf{node}}$ Number of nodes

p Fluid pressure

$\bar{p}$ Boundary pressure

p_{co} Preconsolidation pressure of the modified Cam-clay model

p_i Initial pressure

$\boldsymbol{q}$ Fluid mass flux (fluid mass flow rate per unit area and time)

q' Deviatoric effective stress

$\boldsymbol{s}$ Deviatoric total stress tensor

$\boldsymbol{u}$ Displacement

$\boldsymbol{v}$ Fluid velocity

Δt Time step size

Δx Grid spacing in the x axis

Δz Grid spacing in the z axis

Φ Lagrange's porosity

ϕ True porosity, Euler's porosity

ϕ_p Plastic porosity

$\boldsymbol{\varepsilon}$ Linearized strain tensor

$\boldsymbol{\varepsilon}_p$ Linearized plastic strain tensor

ε_v Volumetric strain (the trace of the strain tensor)

$\varepsilon_{p,v}$ Volumetric plastic strain (the trace of the plastic strain tensor)

φ Test function for flow

γ_{dr} Amplification factor of the drained split

γ_{fc} Amplification factor of the fully coupled method

γ_{sn} Amplification factor of the fixed-strain split

γ_{ss} Amplification factor of the fixed-stress split

γ_{ud} Amplification factor of the undrained split

$\boldsymbol{\eta}$ Test function for mechanics

κ Swell index of the modified Cam-clay model

λ Virgin compression index of the modified Cam-clay model

μ Fluid viscosity

ν Poisson's ratio

θ Phase parameter in the Von Neumann method

ρ_b Bulk density

ρ_f Fluid density

ρ_s Density of the solid phase

$\boldsymbol{\sigma}$ Cauchy total stress tensor

$\boldsymbol{\sigma}'$ Effective stress tensor

$\bar{\sigma}$ Overburden

σ_v Volumetric (mean) total stress

σ'_v Volumetric effective stress

τ Coupling strength

$\mathbf{1}$ Rank-2 identity tensor

$(\cdot)_0$ Reference state

$(\cdot)^d$ Number of space dimensions

$(\cdot)_d$ Dimensionless quantity

$(\cdot)^n$ Time level

$(\cdot)^k$ Iteration level

$\dot{(\,)}$ Time derivative

References

Aavatsmark I. 2002. An introduction to multipoint flux approximations for quadrilateral grids. *Comput Geosci* **6**: 405–432.

Abousleiman A., Cheng A., Detournay E., and Roegiers J. 1996. Mandel's problem revisited. *Geotechnique* **46**: 187–195.

Armero F. 1999. Formulation and finite element implementation of a multiplicative model of coupled poro-plasticity at finite strains under fully saturated conditions. *Comput Methods Appl Mech Eng* **171**: 205–241.

Armero F. and Simo J.C. 1992. A new unconditionally stable fractional step method for non-linear coupled thermomechanical problems. *Int J Numer Methods Eng* **35**: 737–766.

Aziz K. and Settari A. 1979. *Petroleum Reservoir Simulation*. London: Elsevier.

Bevillon D. and Masson R. 2000. Stability and convergence analysis of partially coupled schemes for geomechanics reservoir simulations. Eur Conf Math Oil Recovery, Baveno, Italy.

Biot M.A. 1941. General theory of three-dimensional consolidation. *J Appl Phys* **12**: 155–164.

Borja R.I. 2006. On the mechanical energy and effective stress in saturated and unsaturated porous continua. *Int J Solid Struct* **12**: 1764–1786.

Borja R.I. and Lee S.R. 1990. Cam-clay plasticity, Part I: Implicit integration of elasto-plastic constitutive relations. *Comput Methods Appl Mech Eng* **78**: 49–72.

Coussy O. 1995. *Mechanics of porous continua*. Chichester, England: John Wiley and Sons.

Dean R.H., Gai S., Stone C.M., and Minkoff S.E. 2006. A comparison of techniques for coupling porous flow and geomechanics. *SPE J* **11**(1): 132–140.

Farhat C., Park K.C., and Dubois-Pelerin Y. 1991. An unconditionally stable staggered algorithm for transient finite element analysis of coupled thermoelastic problems. *Comput Methods Appl Mech Eng* **85**: 349–365.

Felippa C.A. and Park K.C. 1980. Staggered transient analysis procedures for coupled mechanical systems: formulation. *Comput Methods Appl Mech Eng* **24**: 61–111.

Fredrich J.T., Arguello J.G., Deitrick G.L., and de Rouffignac E.P. 2000. Geomechanical modeling of reservoir compaction, surface subsidence, and casing damage at the Belridge diatomite field. *SPE Res Eval Eng* **3**(4): 348–359.

Gai X. 2004. A coupled geomechanics and reservoir flow model on parallel computers. Ph.D. Dissertation, University of Texas at Austin.

Gai X., Sun S., Wheeler M.F., and Klie H. 2005. A timestepping scheme for coupled reservoir flow and geomechanics on nonmatching grids. SPE Ann Tech Conf Exhib (SPE 97054), Dallas.

Geertsma J. 1957. The effect of fluid pressure decline on volumetric change of porous rocks. *Trans. AIME* **210**: 331–340.

Huang M. and Zienkiewicz O.C. 1998. New unconditionally stable staggered solution procedures for coupled soil-pore fluid dynamic problems. *Int J Numer Methods Eng* **43**: 1029–1052.

Hughes T.J.R. 1987. *The Finite Element Method: Linear Static and Dynamic Finite Element Analysis*. Englewood Cliffs, NJ: Prentice-Hall.

Jean L., Mainguy M., Masson R., and Vidal-Gilbert S. 2007. Accelerating the convergence of coupled geomechanical-reservoir simulations. *Int J Numer Anal Meth Geomech* **31**: 1163–1181.

Jha B. and Juanes R. 2007. A locally conservative finite element framework for the simulation of coupled flow and reservoir geomechanics. *Acta Geotechnica* **2**: 139–153.

Kim J. 2009. Sequential formulation of coupled geomechanics and multiphase flow. Ph.D. Dissertation, Stanford University. In Progress.

Lewis R.W. and Schrefler B.A. 1998. *The finite element method in the static and dynamic deformation and consolidation of porous media*. Chichester, England: Wiley, 2nd edition.

Lewis R.W. and Sukirman Y. 1993. Finite element modelling of three-phase flow in deforming saturated oil reservoirs. *Int J Numer Anal Meth Geomech* **17**: 577–598.

Li P. and Chalaturnyk R.J. 2005. Geomechanical model of oil sands. SPE Int Therm Oper Heavy Oil Sym (SPE/PS-CIM/CHOA 97949), Dallas, 1-3 Nov.

Mainguy M. and Longuemare P. 2002. Coupling fluid flow and rock mechanics: formulations of the partial coupling between reservoir and geomechanics simulators. *Oil Gas Sci Tech* **57**: 355–367.

Miga M.I., Paulsen K.D., and Kennedy F.E. 1998. Von Neumann stability analysis of Biot's general two dimensional theory of consolidation. *Int J Numer Methods Eng* **43**: 955–974.

Minkoff S.E., Stone C.M., Bryant S., Peszynska M., and Wheeler M.F. 2003. Coupled fluid flow and geomechanical deformation modeling. *J Petrol Sci Eng* **38**: 37–56.

Murad M.A. and Loula A.F.D. 1992. Improved accuracy in finite element analysis of Biot's consolidation problem. *Comput Methods Appl Mech Eng* **95**: 359–382.

Murad M.A. and Loula A.F.D. 1994. On stability and convergence of finite element approximations of Biot's consolidation problem. *Comput Methods Appl Mech Eng* **37**: 645–667.

Park K.C. 1983. Stabilization of partitioned solution procedure for pore fluid-soil interaction analysis. *Int J Numer Methods Eng* **19**(11): 1669–1673.

Phillips P.J. and Wheeler M.F. 2007a. A coupling of mixed and continuous Galerkin finite element methods for poroelasticity I: the continuous in time case. *Comput Geosci* **11**: 131–144.

Phillips P.J. and Wheeler M.F. 2007b. A coupling of mixed and continuous Galerkin finite element methods for poroelasticity II: the discrete-in-time case. *Comput Geosci* **11**: 145–158.

Prevost J.H. 1997. Partitioned solution procedure for simultaneous integration of coupled-field problems. *Commun. numer. meth. engng.* **13**: 239–247.

Samier P. and Gennaro S. 2007. A practical iterative scheme for coupling geomechanics with reservoir simulation. SPE Europec/EAGE (SPE 107077), London, 11-14 Jun.

Settari A. and Mourits F. 1998. A coupled reservoir and geomechanical simulation system. *SPE J* **3**: 219–226.

Settari A. and Walters D.A. 2001. Advances in coupled geomechanical and reservoir modeling with applications to reservoir compaction. *SPE J* **6**(3): 334–342.

Simo J. 1991. Nonlinear stability of the time-discrete variational problem of evolution in nonlinear heat conduction, plasticity and viscoplas-

ticity. *Comput Methods Appl Mech Eng* **88**: 111–131.
Simo J.C. and Hughes T.J.R. 1998. *Computational inelasticity*. Heidelberg: Springer.
Strikwerda J.C. 2004. *Finite Difference Schemes and Partial Differential Equations*. Philadelphia: SIAM.
Thomas L.K., Chin L.Y., Pierson R.G., and Sylte J.E. 2003. Coupled geomechanics and reservoir simulation. *SPE J* **8**(4): 350–358.
Tran D., Nghiem L., and Buchanan L. 2005. Improved iterative coupling of geomechanics with reservoir simulation. SPE Res Simul Sym (SPE 93244), Houston, 31 Jan.-2 Feb.
Tran D., Settari A., and Nghiem L. 2004. New iterative coupling between a reservoir simulator and a geomechanics module. *SPE J* **9**(3): 362–369.
Truty A. and Zimmermann T. 2006. Stabilized mixed finite element formulations for materially nonlinear partially saturated two-phase media. *Comput Methods Appl Mech Eng* **195**: 1517–1546.
Vermeer P.A. and Verruijt A. 1981. An accuracy condition for consolidation by finite elements. *Int J Numer Anal Meth Geomech* **5**: 1–14.
Wan J. 2002. Stabilized finite element methods for coupled geomechanics and multiphase flow. Ph.D. Dissertation, Stanford University.
Wan J., Durlofsky L.J., Hughes T.J.R., and Aziz K. 2003. Stabilized finite element methods for coupled geomechanicsreservoir flow simulations. SPE Res Simul Sym (SPE 79694), Houston, 3-5 Feb.
Wan J., Sarma P., Usadi A.K., and Beckner B.L. 2005. General stability criteria for compositional and black-oil models. SPE Res Simul Sym (SPE 93096), Houston, 31 Jan-2 Feb.
Wheeler M.F. and Gai X. 2007. Iteratively coupled mixed and Galerkin finite element methods for poro-elasticity. *Numer Meth for PDEs* **23**: 785–797.
White A.J. and Borja R.I. 2008. Stabilized low-order finite elements for coupled solid-deformation/fluid-diffusion and their application to fault zone transients. *Comput Methods Appl Mech Eng* **197**: 4353–4366.
Zienkiewicz O.C., Paul D.K., and Chan A.H.C. 1988. Unconditionally stable staggered solution procedure for soil-pore fluid interaction problems. *Int J Numer Methods Eng* **26**(5): 1039–1055.